Octonary Resistance States in $La_{0.7}Sr_{0.3}MnO_3/BaTiO_3/La_{0.7}Sr_{0.3}MnO_3$ Multiferroic Tunnel Junctions

Yue-Wei Yin, Wei-Chuan Huang, Yu-Kuai Liu, Sheng-Wei Yang, Si-Ning Dong, Jing Tao, Yimei Zhu, Qi Li,[*] and Xiao-Guang Li[*]

[*] Prof. X. G. Li, Dr. Y. W. Yin, W. C. Huang, Dr. Y. K. Liu, S. W. Yang, Dr. S. N. Dong
Hefei National Laboratory for Physical Sciences at Microscale, Department of Physics
University of Science and Technology of China
Hefei 230026, P. R. China
E-mail: lixg@ustc.edu.cn

[*] Prof. Q. Li, Dr. Y. W. Yin
Department of Physics
Pennsylvania State University
University Park 16802, USA
E-mail: qil1@psu.edu

Prof. Y. M. Zhu, Dr. J. Tao
Condensed Matter Physics and Materials Science Department
Brookhaven National Laboratory
Upton, New York 11973, USA

[*] Prof. Prof. X. G. Li,
Collaborative Innovation Center of Advanced Microstructures, Nanjing University
Nanjing, 210093, China
E-mail: lixg@ustc.edu.cn

Keywords: multiferroic tunnel junction, tunneling magnetoresistance effect, magnetic anisotropy, information storage

Abstract: General drawbacks of current electronic/spintronic devices are high power consumption and low density storage. A multiferroic tunnel junction (MFTJ), employing a ferroelectric barrier layer sandwiched between two ferromagnetic layers, presents four resistance states in a single device and therefore provides an alternative way to achieve high density memories. Here, we demonstrate an MFTJ device with eight nonvolatile resistance states by further integrating the design of non-collinear magnetization alignments between the

ferromagnetic layers. Through the angle-resolved tunneling magnetoresistance investigations on $La_{0.7}Sr_{0.3}MnO_3/BaTiO_3/La_{0.7}Sr_{0.3}MnO_3$ junctions, it was found that, besides collinear parallel/antiparallel magnetic configurations, the MFTJ shows at least two other stable non-collinear (45° and 90°) magnetic configurations. Combining the tunneling electroresistance effect caused by the ferroelectricity reversal of the $BaTiO_3$ barrier, an octonary memory device is obtained, representing potential applications in high density nonvolatile storage in future.

1. Introduction

Owing to the potential applications in non-volatile memories and field sensors, a tunneling magnetoresistance (*TMR*) effect has received enormous attention since it was first observed in a magnetic tunnel junction (MTJ) consisting of two ferromagnetic layers separated by a thin insulating barrier.[1-3] Generally, the *TMR* effect is associated with the change of relative orientation $\Delta\theta$ ($0° \leq \Delta\theta \leq 180°$) between the magnetizations $\vec{M}_{top}$ and $\vec{M}_{bottom}$ of the top and bottom ferromagnetic layers. Most studies about *TMR* effect are focused on the collinear magnetization configurations, *i.e.* parallel ($\Delta\theta = 0°$) and antiparallel ($\Delta\theta = 180°$) magnetic states. The bi-stable collinear state design is commonly used in MTJs due to the easily obtained uniaxial magnetic anisotropy in ferromagnetic layers, typically by pinning one of them through an additional antiferromagnetic layer.[4] However, the principle of MTJ allows more magnetic states with different *TMR* values by selecting ferromagnetic layers with more easy-axes. Magnetic multi-state memory devices have been demonstrated using in-plane Hall effect in GaMnAs and Fe systems with fourfold anisotropy[5-7] and spin valves[8]. As for MTJs, taking advantages of the cubic magnetocrystalline anisotropy of (Ga, Mn)As with four in-plane magnetic easy axes in <100> directions, the non-collinear alignment of magnetizations ($\Delta\theta \sim 90°$) with different junction resistances were obtained in

(Ga, Mn)As based MTJs,[9, 10] demonstrating a possible mechanism of multi-state memory devices. Recently Cuellar *et al* have observed the non-collinear magnetization configurations in a 10×10 mm^2 $La_{0.7}Ca_{0.3}MnO_3$ (bottom ferromagnetic layer, easy axes along [100] and [$\bar{1}$00])/$PrBa_2Cu_3O_7$/$La_{0.7}Ca_{0.3}MnO_3$ (top ferromagnetic layer, easy axes along <110> directions) trilayer sample by using depth sensitive polarized neutron reflectometry.[11] Furthermore, the number of magnetic states can be further increased, even to continuum by forming stable magnetic multi-domain structures.[12-14]

Recently, another mechanism to increase the number of memory states in an MTJ was proposed by using a ferroelectric material as tunnel barrier, making the device into a multiferroic tunnel junction (MFTJ).[15, 16] The ferroelectric polarization reversal of the ultrathin barrier will change the tunneling current by changing the asymmetry of the electrostatic potential or interface bonding strength of the two interfaces, leading to a change in junction resistance, known as the tunneling electroresistance (*TER*) effect.[15-17] Similar to the multi ferromagnetic domain related multi-states in MTJs,[12-14] multilevel memristor type behavior can be obtained in ferroelectric tunnel junctions (tunnel junctions with ferroelectric barrier) as well by a partial switching of the ferroelectric domains in ferroelectric barrier.[18-20] While for a single domain MFTJ, it will exhibit four resistance states in a single memory unit cell owing to the coexistence of *TMR* and *TER* effects. The experimental evidences have been demonstrated in MFTJs with (Ba, Sr)TiO_3, $BiFeO_3$, or $PbZr_{0.2}Ti_{0.8}O_3$ ferroelectric tunnel barriers.[21-27] Combining these two mechanisms of increasing storage states, the multinary memory devices with an enhanced capacity of information storage may be achieved through integrating the features of non-collinear magnetization alignment with the ferroelectric polarization switching.

Magnetocrystalline anisotropy of (001) oriented $La_{0.7}Sr_{0.3}MnO_3$ thin films under in-plane tensile substrate constraint is of cubic anisotropy with four easy axes along <110> or

<100> directions,[28-31] which depends on the defects and oxygen vacancies.[29] Meanwhile, its easy axes and magneto-anisotropies can be further designed by the shape[29] and substrate steps,[31] resulting in different preferred directions for magnetization and allowing multiple stable or metastable magnetization states. Up till now, the studies on the effect of magnetic anisotropy and the non-collinear magnetic states in manganite based MTJs were limited,[11, 32, 33] and the multinary MFTJ memory devices with more than four states haven't been obtained experimentally.

In this paper, we studied the junction resistances *versus* magnetic fields of $La_{0.7}Sr_{0.3}MnO_3/BaTiO_3/La_{0.7}Sr_{0.3}MnO_3$ MFTJs at different in-plane field angles φ. Because of the different magnetic shape anisotropies, the square top and rectangular bottom $La_{0.7}Sr_{0.3}MnO_3$ layers show fourfold and twofold magnetic anisotropies respectively. An octonary memory device with eight non-volatile resistance states is achieved by manipulating the magnetic configurations of $\vec{M}_{top}$ and $\vec{M}_{bottom}$ as well as reversing the ferroelectric polarization of the $BaTiO_3$ barrier.

2. Results and Discussion

The MFTJs were fabricated from epitaxial $La_{0.7}Sr_{0.3}MnO_3$ (50 nm, bottom ferromagnetic layer)/$BaTiO_3$ (3 nm, ferroelectric barrier layer)/$La_{0.7}Sr_{0.3}MnO_3$ (30 nm, top ferromagnetic layer) heterostructures grown on $SrTiO_3$ (001) substrates by a pulsed laser deposition technique. The schematic drawing of the MFTJ structure is illustrated in **Figure 1**(a). The shapes and thicknesses of the top and bottom ferromagnetic layers were designed to make their magnetic anisotropies different from each other. The magnetic anisotropy of the square $La_{0.7}Sr_{0.3}MnO_3$ top layer (15μm×15μm×30nm) was dominated by the magnetic crystalline anisotropy with its easy axes pointing toward <110> directions and hard axes along <100> directions. The rectangular $La_{0.7}Sr_{0.3}MnO_3$ bottom layer (750μm×30μm×50nm) shows easy axes along <110> directions as well but was designed with longitudinal direction

along [100] axis, making its [010] and [$0\bar{1}0$] hard directions relatively harder and the [100]/ [$\bar{1}00$] hard directions easier.[29] The magnetic anisotropy of the $La_{0.7}Sr_{0.3}MnO_3$ electrodes is consistent with previous reports[28-30] and our angular dependent magnetization measurements by magneto-optical Kerr effect (Supplementary Figure S1).

Structural and chemical characterizations of an as-grown multilayer fabricated under identical conditions as our MFTJ were performed by cross-sectional energy-dispersive X-ray (EDX) spectroscopy and high resolution transmission electron microscopy (HRTEM). Figure 1(b) shows the EDX map of Ti element (colored red) of an as-grown multilayer from the $SrTiO_3$ substrate (left) to the coated Au (right) on top of the trilayer, which confirms the position of $BaTiO_3$ barrier, as indicated by the arrow shown in Figure 1(b). Figure 1(c) is an HRTEM image at the interface region which shows a continuous barrier layer, and the single crystalline quality is indicated by the selected area diffraction pattern shown in the inset of Figure 1(c). Piezoresponse force microscopy measurements have been carried out in our previous work to confirm the ferroelectric nature of $BaTiO_3$ barrier.[26, 34]

To investigate whether different magnetic states exist in this MFTJ device, the magnetic field *H* dependences of resistance *R* at various field orientations were measured at 80 K because the junction resistance will track the relative orientation of the magnetic moments of top and bottom layers due to the spin-conserving nature of tunneling (Supplementary Figure S2).[9, 11, 35] **Figure 2** shows the representative *R*(*H*) curves with the magnetic fields applied along [110] easy axis and [010] hard axis, respectively, with the ferroelectric polarizations of barrier poled upward and downward. Different magneto-electric resistance states are observed and their corresponding magnetization configurations and ferroelectric directions are schematically shown in **Figure 3**.

Figure 2(a) shows *R*(*H*) curve at upward polarization state of $BaTiO_3$ with the magnetic fields sweeping from -600 Oe to +600 Oe and then back to -600 Oe. Both sweeps are

symmetric to each other and we will only discuss the $R(H)$ sweeping from -600 Oe to +600 Oe. Because the magnetic field is along [110] easy axis of both ferromagnetic layers, therefore, the $\vec{M}_{top}$ and $\vec{M}_{bottom}$ can be flipped between [110] and $[\bar{1}\bar{1}0]$ directions to form parallel and antiparallel states. At -600 Oe, the magnetic field aligns both $\vec{M}_{top}$ and $\vec{M}_{bottom}$ to $[\bar{1}\bar{1}0]$ direction (see Figure 3 for illustration) and forms a parallel magnetic state 1 (~8.2 kΩ, $\Delta\theta = 0°$), which is stable and nonvolatile at zero magnetic field. When the reversing magnetic field only overcomes the switching fields of $\vec{M}_{bottom}$ but is still smaller than that of $\vec{M}_{top}$, $\vec{M}_{bottom}$ will be flipped to be antiparallel to $\vec{M}_{top}$ ($\Delta\theta = 180°$, as illustrated in Figure 3), corresponding to the resistance state 3 in Figure 2(a) (~13.4-14.9 kΩ, $\Delta\theta = 180°$). To support the process mentioned above, namely, $\vec{M}_{bottom}$ flips first, the magnetic field dependence of resistance for the $La_{0.7}Sr_{0.3}MnO_3$ bottom lead has been measured by four probe method.[32] The peak of the resistance *vs*. magnetic field curve (data not shown), denoting the average coercive field of the bottom ferromagnetic layer (~50 Oe), appears at a magnetic field close to the switching field from parallel to antiparallel state in Figure 2(a). Therefore, we can ascribe the resistance switching from parallel to antiparallel state to the bottom ferromagnetic layer, and the switching at higher field from antiparallel to parallel state to top ferromagnetic layer. This is consistent with the report on $La_{0.7}Ca_{0.3}MnO_3$ based MTJs,[11, 32] and is supported by the following results.

The highest *TMR* ratio in this MFTJ structure, defined as $TMR = (R_{AP} - R_P)/R_P$, is about 82%, where R_P and R_{AP} are the resistances in the parallel state 1 and antiparallel state 3, respectively. According to Slonczewski's model,[36] the $\Delta\theta$ dependent resistance R of an MTJ is given by

$$R(\Delta\theta) = \frac{R_b}{1 + P^2 \cos\Delta\theta} \tag{1}$$

where R_b is a constant related to the insulating barrier and P is the effective spin polarization of the ferromagnetic-barrier couple. Based on the values of parallel state resistance R_P = 8.2 kΩ with $\Delta\theta$ = 0° and antiparallel state resistance R_{AP} =14.9 kΩ with $\Delta\theta$ = 180°, it can be derived that R_b = 10.6 kΩ and P = 0.54 for the MFTJ at 80 K with upward polarization of $BaTiO_3$.

From Figure 2(a) together with Figure 3, it is also noted that in the middle of the resistance switching from parallel state 1 to antiparallel state 3, the MFTJ experiences an intermediate resistance state 2 (~10.4-10.7 kΩ), for which the $\Delta\theta$ is ~86.6°-92.2°, as calculated using Equation (1), suggesting that the state 2 is of a perpendicular magnetization configuration, corresponding to the rotation of $\vec{M}_{bottom}$ to an intermediate easy axis ($[\bar{1}10]$ direction, as illustrated in Figure 3) before its 180° switching from $[\bar{1}\bar{1}0]$ to [110]. This may be related to the shape anisotropy of the $La_{0.7}Sr_{0.3}MnO_3$ bottom layer with longitudinal direction along [100]/$[\bar{1}00]$, which can reduce the energy barrier between $[\bar{1}\bar{1}0]$ and $[\bar{1}10]$ easy axes and increase the energy barrier between $[\bar{1}10]$ and [110] easy axes, therefore the Zeeman energy at state 2 can be sufficient to flip $\vec{M}_{bottom}$ from $[\bar{1}\bar{1}0]$to $[\bar{1}10]$ but not large enough to keep switching $\vec{M}_{bottom}$ from $[\bar{1}10]$ to [110].

In Figure 2(b), the blue curve displays the minor $R(H)$ loop with magnetic fields sweeping from -600 Oe to +90 Oe and then back to -600 Oe, before the flip of $\vec{M}_{top}$. In this case, only the 180° switching field of $\vec{M}_{bottom}$ is realized, and the MFTJ stays in the antiparallel state 3 (~ 13.7 kΩ) even when the magnetic field is reduced to zero. Furthermore, if we set the turning field to +60 Oe (green curve in Figure 2(b)), the resistance state 2 with $\vec{M}_{top}$ and $\vec{M}_{bottom}$ along different easy axes ($\vec{M}_{bottom} \perp \vec{M}_{top}$) stays stable at zero magnetic field.

The junction resistance of the MFTJ could be further manipulated by ferroelectric polarization of barrier, displaying *TER* effect.[21-26] For the MFTJ, the ferroelectric

polarization of the $BaTiO_3$ barrier can be aligned downward or upward by a poling voltage of +1.5 V or -1.5 V. As shown in **Figure 4**, by a series of consecutive switching of the barrier polarization, the parallel resistances between the two polarization states 1 and 4 can be switched each other directly. To exclude other resistance switching mechanisms such as the interfacial electrochemical modification or conducting filament formation and rupture[37, 38], piezoresponse force microscopy has been carried out to demonstrate that the ferroelectric polarization reversal is the underlying mechanism for the *TER* resistive switching in our system (Supplementary Figure S3).[34] As shown in Figure 2(c) and 2(d), the *R*(*H*) curves and corresponding minor loops with *H*//[110] are displayed after reversing the ferroelectric polarization of barrier from upward to downward direction, which are similar to those observed with ferroelectric polarization pointing upward. However, owing to the *TER* effect, the parallel state 4, perpendicular state 5, and antiparallel state 6 with $BaTiO_3$ polarized downward show larger resistances than the corresponding magnetic states 1, 2, and 3 at upward state.

When the magnetic field is applied along the hard axis, the magnetization flipping between two hard axes will pass through its easy axes, therefore other non-collinear magnetic states will appear, as shown in Figure 2(e) for *H*//[010] which is the hard axis of both top and bottom $La_{0.7}Sr_{0.3}MnO_3$ layers. The most curious behavior is that, besides the two parallel states at -600 Oe and +600 Oe, the MFTJ experiences another parallel state 1" between two high resistance states 7 and 7'. This is very different from ordinary MTJs with only one parallel and one antiparallel states between 0 Oe and 600 Oe, which could happen only when the $\vec{M}_{top}$ and $\vec{M}_{bottom}$ both show multi steps flipping and rotate one by one to the same easy axis before their complete magnetization reversals. We can take the field scan from -600 Oe to +600 Oe as an example. At first, the field of -600 Oe forces $\vec{M}_{top} // \vec{M}_{bottom} // [0\bar{1}0]$ forming parallel state 1′ (see Figure 3), and this parallel state 1′ survives at zero field with stable

resistance. However, the MFTJ leaves parallel state 1′ at 10 Oe which is much smaller than that for state 1 in Figure 2(a) (~30 Oe). This is because $[0\bar{1}0]$ is a hard axis for the $La_{0.7}Sr_{0.3}MnO_3$ bottom layer in which the elongated direction is perpendicular to $[0\bar{1}0]$ and therefore a smaller field is needed to flip $\vec{M}_{bottom}$ away from $[0\bar{1}0]$ axis. A resistance state 7 of 8.8-8.9 kΩ is reached at 32 Oe, with $\Delta\theta \sim$ 46-49° as calculated by using Equation (1), indicating that the $\vec{M}_{bottom}$ may point to $[1\bar{1}0]$ or $[\bar{1}\bar{1}0]$ easy axis (which axis is preferred may be related to the very small misalignment of magnetic field to $[0\bar{1}0]$) with $\vec{M}_{top}$ staying in $[0\bar{1}0]$ direction. Here, the switching of $\vec{M}_{bottom}$ to $[\bar{1}\bar{1}0]$ is used in Figure 3. And due to the energy barrier between $[\bar{1}\bar{1}0]$ and $[\bar{1}10]$, $\vec{M}_{bottom}$ switches to $[\bar{1}\bar{1}0]$ but not $[\bar{1}10]$ at 10 Oe, forming the 45° state shown as state 7 in Figure 3.

With further increasing magnetic fields, the magnetization of top layer switches away from the $[0\bar{1}0]$ hard axis as well. At 110 Oe, both $\vec{M}_{bottom}$ and $\vec{M}_{top}$ are switched to $[\bar{1}10]$ easy axis, leading to another parallel state 1″ (illustrated in Figure 3). After then, $\vec{M}_{bottom}$ and $\vec{M}_{top}$ rotate away from the $[\bar{1}10]$ easy axis to be close to external field direction (H//[010]). As we know, the magnetization of a magnetic material will rotate a small angle away from easy axis toward magnetic field direction, and the rotation angle depends on the anisotropic energy and Zeeman energy.[9, 39, 40] Therefore, $\vec{M}_{bottom}$ rotates earlier than $\vec{M}_{top}$, and another high resistance state 7′ (~8.8 kΩ, $\Delta\theta \sim$ 45°) is observed at ~195 Oe. With further increasing field, $\vec{M}_{bottom}$ and $\vec{M}_{top}$ will be aligned to [010] hard axis smoothly and reach parallel state above 420 Oe with $\vec{M}_{top} // \vec{M}_{bottom}$//[010]. It is also noted that there are several kinks in the $R(H)$ of Figure 2(e), which should be related to the multi-step jumps of $\vec{M}_{bottom}$ or $\vec{M}_{top}$ toward [010] field direction through <110> easy axes at different magnetic fields.

Figure 2(f) shows the minor loop by setting the turning field at 65 Oe, which confirms the non-volatility of magnetic state 7 with $\Delta\theta \sim 45°$. Figure 2(g) and 2(h) shows the $R(H)$ curves and corresponding minor loop with the ferroelectric polarization of barrier pointing downward. The nonvolatile 45° magnetic state 8 at downward polarization state show larger resistance than that of upward. The minor hysteresis loop scans by setting different turning fields to reach resistance states 1″ and 7′ were also measured. Figure 2(i) shows the $R(H)$ minor loop with turning field at 130 Oe at which the MFTJ is in parallel state 1″, which shows a similar shape to normal MTJ device (Figure 1(a)). Figure 2(j) shows the minor loop by setting the turning field at 230 Oe at magnetic state 7′. As the field is reduced, the resistance for this state gradually increases to state 2′, due to the relaxation of the two magnetizations toward their respective easy axes, which increases the angle between them. At zero magnetic field, the non-volatile state 2′ with resistance of ~10 kΩ, $\Delta\theta \sim 78°$ close to perpendicular configuration is obtained. Although with similar resistance and $\Delta\theta$, the perpendicular configuration 2′ (see Figure 3) is different from the state 2 obtained in Figure 2(a). The not ideally perpendicular of state 2′ may due to two aspects: 1) the magnetization may be pinned between the easy axes and original position; 2) the magnetizations rotate to more than one easy axis during the magnetization relax back.[11] Similar $R(H)$ minor loops with downward ferroelectricity are shown in Figure 2(k) and 2(l), which show larger resistance than upward. The Supplementary Figure S4 summarizes the switching fields at different field orientations φ by intervals of 5°.

The magnetization configurations discussed above are all determined from the resistance, rotation direction and magnetization reversal mechanism, and there may exist other possible magnetization configurations to explain the data. Although the exact magnetization configurations still need to be confirmed by further experimental studies including real time local magnetic measurement,[11] at least four stable nonvolatile magnetic states and corresponding resistance states with $\Delta\theta \sim 0°$, ~ 45°, ~ 90° and ~ 180° can be obtained. With

ferroelectric pointing upward and downward, we can realize two sets of four nonvolatile magnetic states. We summarized these eight nonvolatile resistance states in **Figure 5** which shows distinct resistance differences from each other. From Figure 5, the switching procedures between these states can also be realized by magnetic and electric fields. Data retention up to 30 min is shown in Supplementary Figure S5. It should be pointed out that the octonary resistance states in our MFTJs is related to the non-collinear magnetization alignments and the ferroelectric polarization switching of the barrier. While the multi-states in the MTJ/FTJ memristors[12-14, 18-20] are related to the ferromagnetic/ferroelectric domain nucleation and growth by varying the reversing magnetic/electric fields amplitude. It is obviously different between these two kinds of memory devices, and our design shows potential applications in reliable high-density memory.

For designing a memory cell in our MFTJ, a reading wire can be used for electric polarization writing, while the drawback is that two writing wires are needed to apply magnetic fields along different directions ([110] and [010]). In this case, our MFTJ prototype octonary memory unit (0, 1, 2, 3, 4, 5, 6, 7) can be designed to display the eight magnetoelectric storage states in binary memory (000, 001, 010, 011, 100, 101, 110, and 111), as shown in **Table 1**. One octonary memory unit can be used to replace three normal binary memory units and the space in between, which significantly increases the memory density and reduces the dimension of memory device. The switching procedures for any state by a combination of electric and magnetic fields are also shown in Table 1. For example, a procedure of -1.5V, -600 $Oe_{[110]}$, +90 $Oe_{[110]}$ is needed to reach state 3 (3), from any arbitrary state. Only a -1.5V is needed to switch state 6 (7) to state 3 (3). Representative switchings of the junction resistances among different states by different combinations of electric and magnetic fields are shown in the supplementary Figure S6. Furthermore, it should be mentioned that the *TMR* and *TER* ratios reduce with increasing temperature and the *TMR* effect disappears above ~200 K. Although further studies on material selection and interface

engineering are needed to optimize the device characteristics and obtain room temperature effect, our results provide a concept for alternating way to achieve high density non-volatile memory devices.

3. Conclusions

To summarize, we have studied the angle dependent *TMR* effect of the $La_{0.7}Sr_{0.3}MnO_3/BaTiO_3/La_{0.7}Sr_{0.3}MnO_3$ MFTJ with square top layer and rectangular bottom layer. Besides parallel ($\Delta\theta \sim 0°$) and antiparallel ($\Delta\theta \sim 180°$) states, the nonvolatile non-collinear magnetic configurations with $\Delta\theta \sim 45°$ and 90° between the magnetic layers were also realized and their spin alignments were carefully identified through the angular dependent magnetoresistance data obtained at different field orientations. More significantly, the eight nonvolatile magneto-electric states are obtained in a single device, which offers a new approach for multi-stable resistive devices with promising applications in nanoelectronics and data storage.

4. Experimental Section

Sample Preparation: The $La_{0.7}Sr_{0.3}MnO_3$ (50 nm, bottom layer)/$BaTiO_3$ (3 nm)/$La_{0.7}Sr_{0.3}MnO_3$ (30 nm, top layer) multilayer heterostructures were epitaxially grown by pulsed laser deposition (KrF laser 248 nm) onto (001)-oriented $SrTiO_3$ substrates at a deposition temperature of 750 °C in a flowing oxygen atmosphere of 300 mTorr. After cooling down to room temperature, Cr/Au layer was grown by *dc* magnetron sputtering on the top of the multilayer for making electrical contacts later on. The micron-scale junction in the cross-strip geometry was patterned by a three-step photolithography and Ar ion milling to define the $La_{0.7}Sr_{0.3}MnO_3$ bottom lead, junction area, and the top Au lead, respectively. SiO_2 deposited by RF sputtering was used to isolate the bottom $La_{0.7}Sr_{0.3}MnO_3$ layer from the top gold lead contacting with the top layer.

Measurements: The electrical transport properties performed in a Quantum Design PPMS system were characterized by a four-probe method, and the positive bias is defined such that the current flows from the top to the bottom layer. Constant voltage bias (10 mV) was used with an automatic feedback loop turned on to ensure a constant voltage drop across the junction through the voltage leads. The magnetic field H was applied in the plane of the film, with the angle φ between the applied magnetic field H and the longitudinal direction of the bottom $La_{0.7}Sr_{0.3}MnO_3$ lead, *i.e.*, [100] direction (see Figure 1(a) for illustration). The electrical measurement results shown in the paper were from a junction with the size of top layer of 15×15 μm^2, the size of bottom layer of 750×30 μm^2 and the nominal barrier thickness of 3 nm. High resolution transmission electron microscopy (HRTEM) and energy-dispersive X-ray (EDX) spectroscopy have been conducted for structural and chemical characterization of the selected multilayer by using an abberation-corrected JEOL ARM microscope (200 kV) at Brookhaven National Laboratory (BNL). HRTEM images and EDX elemental mapping results were obtained from a cross-sectional multilayer sample.

Supporting Information

Supporting Information is available from the Wiley Online Library.

Acknowledgements

This work at USTC was supported in part by the NSFC, the NBRPC (2012CB922003, 2015CB921201), the FRFCU (WK2030020026) and the CPSF (2014T70590). The work at PSU was supported in part by the DOE (DE-FG02-08ER4653) and the NSF (DMR-1207474 and DMR-1411166). The PSU NNIN Nanofabrication facilities are acknowledged. Work done at BNL was supported by the DOE (DE-AC02-98CH10886).

Received: ((will be filled in by the editorial staff))

Revised: ((will be filled in by the editorial staff))

Published online: ((will be filled in by the editorial staff))

[1] M. Julliere, *Phys. Lett. A* **1975**, *54*, 225.

[2] J.S. Moodera, L.R. Kinder, T.M. Wong, R. Meservey, *Phys. Rev. Lett.* **1995**, *74*, 3273.

[3] S.S.P. Parkin, C. Kaiser, A. Panchula, P.M. Rice, B. Hughes, M. Samant, S.H. Yang, *Nat. Mater.* **2004**, *3*, 862.

[4] S.S.P. Parkin, K.P. Roche, M.G. Samant, P.M. Rice, R.B. Beyers, R.E. Scheuerlein, E.J. O'Sullivan, S.L. Brown, J. Bucchigano, D.W. Abraham, Y. Lu, M. Rooks, P.L. Trouilloud, R.A. Wanner, W.J. Gallagher, *J. Appl. Phys.* **1999**, *85*, 5828.

[5] W.L. Lim, X. Liu, K. Dziatkowski, Z. Ge, S. Shen, J.K. Furdyna, M. Dobrowolska, *Phys. Rev. B* **2006**, *74*, 045303.

[6] S. Lee, D.Y. Shin, S.J. Chung, X. Liu, J.K. Furdyna, *Appl. Phys. Lett.* **2007**, *90*, 152113.

[7] T. Yoo, S. Khym, S.Y. Yea, S. Chung, S. Lee, X. Liu, J.K. Furdyna, *Appl. Phys. Lett.* **2009**, *95*, 202505.

[8] G. Xiang, B.L. Sheu, M. Zhu, P. Schiffer, N. Samarth, *Phys. Rev. B* **2007**, *76*, 035324.

[9] T. Yoo, S. Khym, h. Lee, S. Lee, S. Lee, X. Liu, J.K. Furdyna, D.U. Lee, E.K. Kim, *Appl. Phys. Lett.* **2013**, *102*, 212404.

[10] M. Tanaka, Y. Higo, *Physica E* **2002**, *13*, 495.

[11] F.A. Cuellar, Y.H. Liu, J. Salafranca, N. Nemes, E. Iborra, G. Sanchez-Santolino, M. Varela, M.G. Hernandez, J.W. Freeland, M. Zhernenkov, M.R. Fitzsimmons, S. Okamoto, S.J. Pennycook, M. Bibes, A. Barthelemy, S.G.E. te Velthuis, Z. Sefrioui, C. Leon, J. Santamaria, *Nat. Commun.* **2014**, *5*, 4215.

[12] T. Yoo, S. Lee, X.Y. Liu, J.K. Furdyna, D.U. Lee, E.K. Kim, *IEEE Trans. Magn.* **2014**, *50*, 4401104.

[13] Y.Y. Fang, R.K. Dumas, T.N.A. Nguyen, S.M. Mohseni, S. Chung, C.W. Miller, J. Akerman, *Adv. Funct. Mater.* **2013**, *23*, 1919.

[14] S. Khym, T. Yoo, H. Lee, S. Lee, S. Lee, X.Y. Liu, J.K. Furdyna, D.U. Lee, E.K. Kim, *Appl. Phys. Express* **2012**, *5*, 093004.

[15] E.Y. Tsymbal, H. Kohlstedt, *Science* **2006**, *313*, 181.

[16] E.Y. Tsymbal, A. Gruverman, V. Garcia, M. Bibes, A. Barthelemy, *MRS Bull.* **2012**, *37*, 138.

[17] V. Garcia, M. Bibes, *Nat. Commun.* **2014**, *5*, 4289.

[18] A. Chanthbouala, V. Garcia, R.O. Cherifi, K. Bouzehouane, S. Fusil, X. Moya, S. Xavier, H. Yamada, C. Deranlot, N.D. Mathur, M. Bibes, A. Barthelemy, J. Grollier, *Nat Mater* **2012**, *11*, 860.

[19] D.J. Kim, H. Lu, S. Ryu, C.W. Bark, C.B. Eom, E.Y. Tsymbal, A. Gruverman, *Nano Lett.* **2012**, *12*, 5697.

[20] H. Yamada, V. Garcia, S. Fusil, S. Boyn, M. Marinova, A. Gloter, S. Xavier, J. Grollier, E. Jacquet, C. Carretero, C. Deranlot, M. Bibes, A. Barthelemy, *ACS Nano* **2013**, *7*, 5385.

[21] Y.K. Liu, Y.W. Yin, S.N. Dong, S.W. Yang, T. Jiang, X.G. Li, *Appl. Phys. Lett.* **2014**, *104*, 043507.

[22] Y.W. Yin, M. Raju, W.J. Hu, X.J. Weng, X.G. Li, Q. Li, *J. Appl. Phys.* **2011**, *109*, 07D915.

[23] M. Hambe, A. Petraru, N.A. Pertsev, P. Munroe, V. Nagarajan, H. Kohlstedt, *Adv. Funct. Mater.* **2010**, *20*, 2436.

[24] V. Garcia, M. Bibes, L. Bocher, S. Valencia, F. Kronast, A. Crassous, X. Moya, S. Enouz-Vedrenne, A. Gloter, D. Imhoff, C. Deranlot, N.D. Mathur, S. Fusil, K. Bouzehouane, A. Barthelemy, *Science* **2010**, *327*, 1106.

[25] D. Pantel, S. Goetze, D. Hesse, M. Alexe, *Nat. Mater.* **2012**, *11*, 289.

[26] Y.W. Yin, M. Raju, W.J. Hu, X.J. Weng, K. Zou, J. Zhu, X.G. Li, Z.D. Zhang, Q. Li, *Front. Phys.* **2012**, *7*, 380.

[27] Y.W. Yin, M. Raju, W.J. Hu, J.D. Burton, Y.M. Kim, A.Y. Borisevich, S.J. Pennycook, S.M. Yang, T.W. Noh, A. Gruverman, X.G. Li, Z.D. Zhang, E.Y. Tsymbal, Q. Li, *J. Appl. Phys.* **2015**, *117*, 172601.

[28] K. Steenbeck, R. Hiergeist, *Appl. Phys. Lett.* **1999**, *75*, 1778.

[29] I. Pallecchi, A. Gadaleta, L. Pellegrino, G.C. Gazzadi, E. Bellingeri, A.S. Siri, D. Marre, *Phys. Rev. B* **2007**, *76*, 174401.

[30] P. Lecoeur, P.L. Trouilloud, G. Xiao, A. Gupta, G.Q. Gong, X.W. Li, *J. Appl. Phys.* **1997**, *82*, 3934.

[31] P. Perna, C. Rodrigo, E. Jimenez, F.J. Teran, N. Mikuszeit, L. Mechin, J. Camarero, R. Miranda, *J. Appl. Phys.* **2011**, *110*, 013919.

[32] M.H. Jo, N.D. Mathur, J.E. Evetts, M.G. Blamire, *Appl. Phys. Lett.* **2000**, *77*, 3803.

[33] R. Werner, A.Y. Petrov, L.A. Mino, R. Kleiner, D. Koelle, B.A. Davidson, *Appl. Phys. Lett.* **2011**, *98*, 162505.

[34] Y.W. Yin, J.D. Burton, Y.M. Kim, A.Y. Borisevich, S.J. Pennycook, S.M. Yang, T.W. Noh, A. Gruverman, X.G. Li, E.Y. Tsymbal, Q. Li, *Nat. Mater.* **2013**, *12*, 397.

[35] H. Jaffrès, D. Lacour, F. Nguyen Van Dau, J. Briatico, F. Petroff, A. Vaurès, *Phys. Rev. B* **2001**, *64*, 064427.

[36] J.C. Slonczewski, *Phys. Rev. B* **1989**, *39*, 6995.

[37] H. Kohlstedt, A. Petraru, K. Szot, A. Rudiger, P. Meuffels, H. Haselier, R. Waser, V. Nagarajan, *Appl. Phys. Lett.* **2008**, *92*, 062907.

[38] Y.P. Yao, Y.K. Liu, S.N. Dong, Y.W. Yin, S.W. Yang, X.G. Li, *Appl. Phys. Lett.* **2012**, *100*, 193504.

[39] Z.-H. Wang, G. Cristiani, H.U. Habermeier, *Appl. Phys. Lett.* **2003**, *82*, 3731.

[40] H. Boschker, J. Kautz, E.P. Houwman, G. Koster, D.H.A. Blank, *J. Appl. Phys.* **2010**, *108*, 103906.

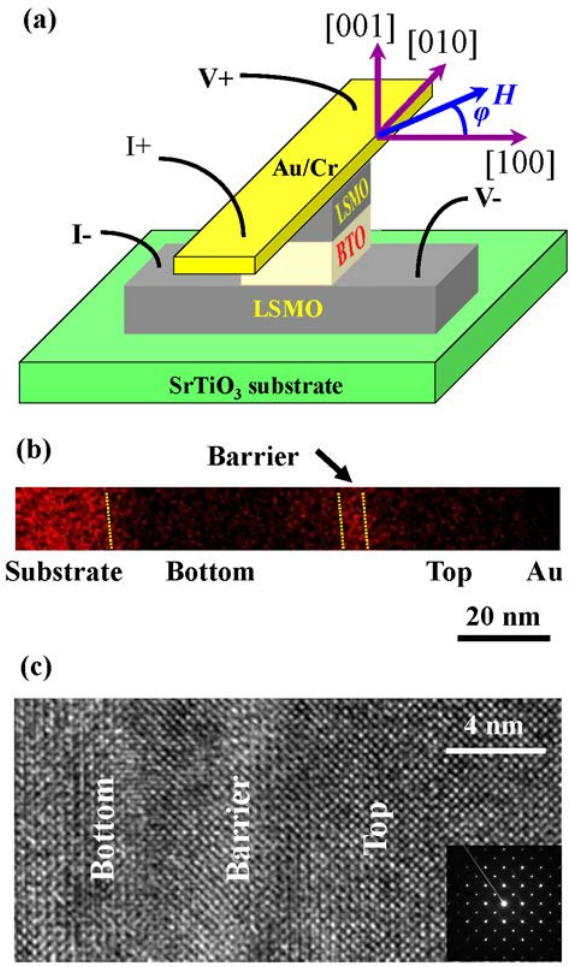

Figure 1. Device geometry, EDX and HRTEM of the MFTJ. (a) The schematic diagram of the MFTJ geometry. (b) the EDX map of Ti element of an as-grown multilayer from the $SrTiO_3$ substrate (left), bottom $La_{0.7}Sr_{0.3}MnO_3$ (LSMO), $BaTiO_3$ barrier, top LSMO, to the coated Au (right) on the top of the trilayer. Yellow dotted lines denotes the positions of interface. (c) The cross-sectional HRTEM image at the interface region of an as-grown multilayer, and the inset is the corresponding diffraction pattern.

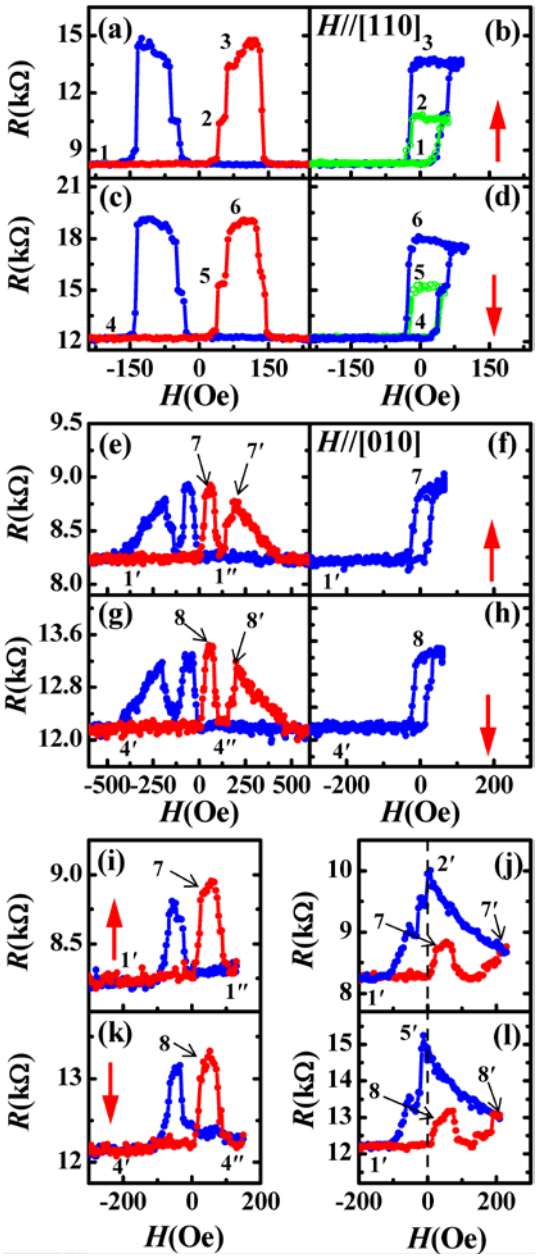

Figure 2. Magnetic field dependence of tunneling resistance of the MFTJ at 80 K. (a)-(d), H//[110]; (e)-(l), H//[010]. The Arabic numerals 1, 1′, 1″, 2, 2′, 3, 4, 4′, 4″, 5, 5′, 6, 7, 7′, 8, and 8′ denotes different magnetoelectric states. The red arrows illustrate the ferroelectric polarization direction of $BaTiO_3$ barrier.

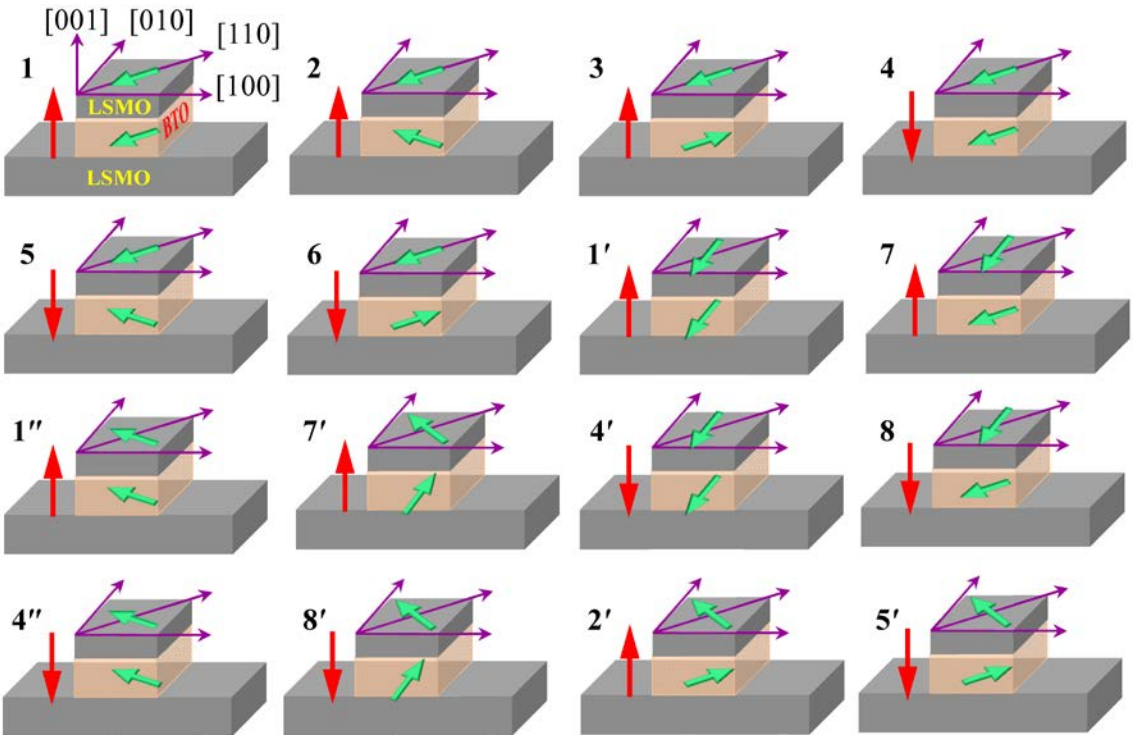

Figure 3. Magnetic configuration and ferroelectric polarization of the different magnetoelectric states observed in Figure 2. The green arrows indicate schematically the directions of the magnetizations of the top and bottom $La_{0.7}Sr_{0.3}MnO_3$ electrodes in plane. The red arrows illustrate the ferroelectric polarization direction of $BaTiO_3$ barrier.

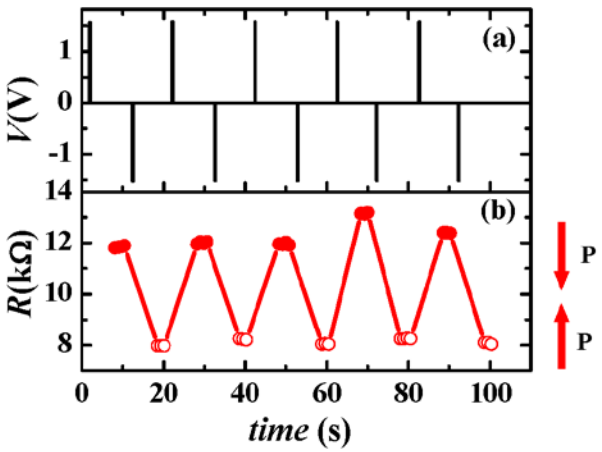

Figure 4. Switching of the junction resistance between states 1 and 4 in response to the applied voltage pulses at a parallel state at 80 K. (a) The applied voltage pulses. (b) Response of the MFTJ resistance. The red arrows indicate the directions of the ferroelectricity poled downward and upward.

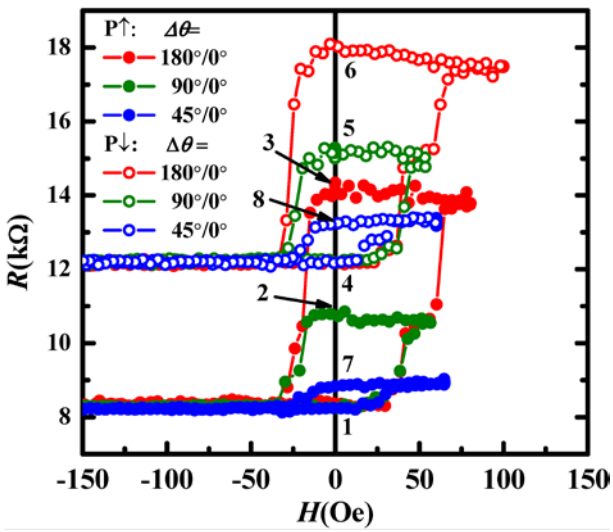

Figure 5. Resistance memory loops as a function of magnetic field showing eight nonvolatile resistance states at 80 K. The Arabic numerals 1, 2, 3, 4, 5, 6, 7, and 8 denotes different resistance states which magnetoelectric configurations are discussed in Figure 2 and 3.

Table 1. Schematic illustrations of the encoding states (binary and octonary) for the MFTJ at different magnetoelectric states with ferroelectric polarization upward (P_{Up}) or downward (P_{Down}) and relative orientation between $\vec{M}_{top}$ and $\vec{M}_{bottom}$ $\Delta\theta$ ~ 0°, 45°, 90° or 180°. The combination of electric and magnetic fields to achieve any state from an arbitrary state is also displayed.

$\Delta\theta$~		0°	45°	90°	180°
P_{Up} (-1.5V)	Binary	**000**	**001**	**010**	**011**
	Octonary	**0**	**1**	**2**	**3**
	Magnetic Field (Oe)	$-600_{[110]}$	$-600_{[010]}$ $+65_{[010]}$	$-600_{[110]}$ $+60Oe_{[110]}$	$-600_{[110]}$ $+90_{[110]}$
P_{Down} (+1.5V)	Binary	**100**	**101**	**110**	**111**
	Octonary	**4**	**5**	**6**	**7**
	Magnetic Field (Oe)	$-600_{[110]}$	$-600_{[010]}$ $+65_{[010]}$	$-600_{[110]}$ $+60_{[110]}$	$-600_{[110]}$ $+90_{[110]}$

Table of contents entry

Comining the ferroelectric orientation (up and down) in the $BaTiO_3$ barrier as well as different non-volatile magnetic configurations ($\Delta\theta$ ~ 0°, 45°, 90°, and 180°) between the ferromagnetic $La_{0.7}Sr_{0.3}MnO_3$ electrodes, eight nonvolatile memory states are obtained in a single multiferroic tunnel junction device, providing a new approach for multi-stable resistive devices with promising applications in nanoelectronics and data storage.

Keyword

multiferroic tunnel junction, tunneling magnetoresistance effect, magnetic anisotropy, information storage

Octonary resistance states in $La_{0.7}Sr_{0.3}MnO_3/BaTiO_3/La_{0.7}Sr_{0.3}MnO_3$ multiferroic tunnel junctions

Yue-Wei Yin, Wei-Chuan Huang, Yu-Kuai Liu, Sheng-Wei Yang, Si-Ning Dong, Jing Tao, Yimei Zhu, Qi Li, and Xiao-Guang Li**

ToC figure:

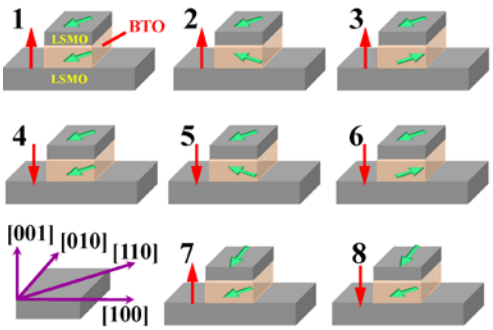

Octonary Memory States